One-Pot Synthesis of Block Copolymer Coated Cobalt Nanocrystals

Guojun Liu,* Xiaohu Yan, Zhihua Lu, Scott A. Curda, and Jyotsana Lal

Department of Chemistry, Queen's University, 90 Bader Lane, Kingston, Ontario, Canada K7L 3N6

Received May 17, 2005. Revised Manuscript Received July 25, 2005

Reported in this paper is the preparation of ϵ-Co nanocrystals coated by a monolayer of poly(acrylic acid)-*block*-polystyrene or PAA−PS. This method is adopted from one using oleic acid as the surfactant. The replacement of oleic acid by PAA−PS as the surfactant during Co nanoparticle preparation yields Co/PAA−PS particles that can be solvent-cast to yield bulk films. For the multidentate nature of the PAA binding block, the PAA−PS coating is resistant toward solvent rinsing. The thickness of the coating can be increased by increasing the length of the PS block.

I. Introduction

Co superparamagentic nanoparticles are prepared generally by cobalt salt reduction or $Co(CO)_8$ thermal decomposition in the presence of a low-molar-mass surfactant or surfactants.[1−3] The resultant Co particles are coated by a low-molar-mass surfactant with potential applications in immunoassay,[4] electric devices,[5] electromagnetic shielding,[1b,6] and information storage.[7] For applications such as high-density information storage, Co nanoparticles coated by polymers are more desirable because such devices will most likely be embodied in the form of a film containing ordered Co nanoparticles. This paper reports the adoption of a simple one-pot synthesis method originally developed by Sun, Murray, and coworkers[2] using low-molar-mass surfactants for the production of polymer-coated Co nanocrystals. This involves the high-temperature reduction of cobalt acetate in the presence of poly(acrylic acid)-*block*-polystyrene (PAA−PS):

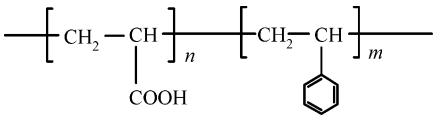

PAA-PS

The preparation of polymer-coated Co nanoparticles is not without precedents. Co nanoparticles have, for example, been prepared in the poly(4-vinyl pyridine) cores of the spherical micelles of polystyrene-*block*-poly(4-vinyl pyridine) or PS−PVP.[8] This involved typically three steps consisting of micelle preparation, Co^{2+} loading into the micellar cores, and then Co^{2+} reduction. For cases when Co^{2+} was reduced at room temperature, several Co particles were often produced within each micelle core. Co nanoparticles have also been produced in the ionic domains of a Nafion membrane.[9] The size distribution of such particles was wide.

Besides Co nanoparticles, the block copolymer template approach has been used to make nanoparticles of other metals including Au, Pd, and Pt as well as metal oxides and semiconductors.[10−16] Such templates can be the cores of block copolymer micelles formed in a block-selective

* To whom correspondence should be addressed. E-mail: guojun.liu@chem.queensu.ca.

(1) (a) Hyeon, T. *Chem. Commun.* **2003**, 927. (b) Leslie-Pelecky, D. L.; Rieke, R. D. *Chem. Mater.* **1996**, *8*, 1770.
(2) (a) Sun, S. H.; Murray, C. B. *J. Appl. Phys.* **1999**, *85*, 4325. (b) Murray, C. B.; Sun, S. H.; Gaschler, W.; Betley, T. A.; Kagan, C. R. *IBM J. Res., Dev.* **2001**, *45*, 47. (c) Wang, Z. L.; Dai, Z. R.; Sun, S. H. *Adv. Mater.* **2000**, *12*, 1944.
(3) (a) Puntes, V. F.; Krishnan, K. M.; Alivisatos, P. *Appl. Phys. Lett.* **2001**, *78*, 2187. (b) Dinega, D. P.; Bawendi, M. G. *Angew. Chem., Int. Ed.* **1999**, *38*, 1788. (c) Shafi, K. V. P. M.; Gedanken, A.; Prozorov, R. *Adv. Mater.* **1998**, *10*, 590. (d) Puntes, V. F.; Krishnan, K. M.; Alivisatos, A. P. *Science* **2001**, *291*, 2115.
(4) (a) Bamnolker, H.; Nitzan, B.; Gura, S.; Margel, S. *J. Mater. Sci. Lett.* **1997**, *16*, 1412. (b) Kondo, A.; Kamura, H.; Higashitani, K. *Appl. Microbiol. Biotechnol.* **1994**, *41*, 99. (c) Yen, S. P. S.; Rembaum, A. *Nature* **1977**, *268*, 437.
(5) Black, C. T.; Murray, C. B.; Sandstrom, R. L.; Sun, S. H. *Science* **2000**, *290*, 1131.
(6) Schnur, J. M. *Science* **1993**, *262*, 1669.
(7) Weller, D.; Sun. S. H.; Murray, C.; Folks, L.; Moser, A. *IEEE Trans. Magnet.* **2001**, *37*, 2185.
(8) (a) Platonova, O. A.; Bronstein, L. M.; Solodovnikov, S. P.; Yanovskaya, I. M.; Obolonkova, E. S.; Valetsky, P. M.; Wenz, E.; Antonietti, M. *Colloid Polym. Sci.* **1997**, *275*, 426−31. (b) Boyen, H. G.; Kastle, G.; Zurn, K.; Herzog, T.; Weigl, F.; Ziemann, P.; Mayer, O.; Jerome, C.; Moller, M.; Spatz, J. P.; Garnier, M. G.; Oelhafen, P. *Adv. Funct. Mater.* **2003**, *13*, 359. (c) Lin, X. M.; Sorensen, C. M.; Klabunde, K. J.; Hajipanayis, G. C. *J. Mater. Res.* **1999**, *14*, 1542. (d) Rutnakornpituk, M.; Thompson, M. S.; Harris, L. A.; Farmer, K. E.; Esker, A. R.; Riffle, J. S.; Conolly, J.; St. Pierre, T. G. *Polymer* **2002**, *43*, 2337. (e) Tadd, E. H.; Bradley, J.; Tannenbaum, R. *Langmuir* **2002**, *18*, 2378.
(9) (a) Park, I. W.; Yoon, M.; Kim, Y. M.; Kim, Y.; Kim, J. H.; Kim, S.; Volkov, V. *J. Magnet. Magnet. Mater.* **2004**, *272−276*, 1413. (b) Leslie-Pelecky, D. L.; Zhang, X. Q.; Rieke, R. D. *J. Appl. Phys.* **1996**, *79*, 5312.
(10) (a) Forster, S.; Antonietti, M. *Adv. Mater.* **1998**, *10*, 195. Klingelhofer, S.; Heitz, W.; Greiner, A.; Oesreich, S.; Forster, S.; Antonietti, M. *J. Am. Chem. Soc.* **1997**, *119*, 10116. (c) Segregina, M. V.; Bronstein, L. M.; Platonova, O. A.; Chernyshov, D. M.; Valetsky, P. M.; Hartmann, J.; Wenz, E.; Antonietti, M. *Chem. Mater.* **1997**, *9*, 923.
(11) (a) Mossmer, S.; Spatz, J. P.; Moller, M.; Aberle, T.; Schmidt, J.; Burchard, W. *Macromolecules* **2000**, *33*, 4791. (b) Selvan, S. T.; Hayakawa, T.; Nogami, M.; Moller, M. *J. Phys. Chem. B* **1999**, *103*, 7441.
(12) Moffit, M.; Vali, H.; Eisenberg, A. *Chem. Mater.* **1998**, *10*, 1021.
(13) For examples on the preparation of metal and metal oxide particles inside the core of cross-linked cylindrical or spherical micelles see (a) Li, Z.; Liu, G. J. *Langmuir* **2003**, *19*, 10480. (b) Yan, X. H.; Liu, G. J.; Liu, F. T. *Angew. Chem., Int. Ed.* **2001**, *40*, 3593. (c) Underhill, R. S.; Liu, G. J. *Chem. Mater.* **2000**, *12*, 3633. (d) Underhill, R. S.; Liu, G. J. *Chem. Mater.* **2000**, *12*, 2082.
(14) Horiuchi, S.; Fujta, T.; Hayakawa, T.; Nakao, Y. *Langmuir* **2003**, *19*, 2963.
(15) (a) Chan, Y. N. C.; Schrock, R. R.; Cohen, R. E. *J. Am. Chme. Soc.* **1992**, *114*, 7295. (b) Kane, R. S.; Cohen, R. E.; Silbey, R. *Chem. Mater.* **1999**, *11*, 90. (c) Kane, R. S.; Cohen, R. E.; Silbey, R. *Chem. Mater.* **1996**, *8*, 1919.

10.1021/cm051050b CCC: $30.25
Published on Web 09/02/2005

Table 1. Characteristics of P*t*BA−PS

sample	SEC M_w/M_n	SEC M_w	NMR n/m[a]	m
P*t*BA−PS_6	1.23	4300	3.5	6
P*t*BA−PS_{25}	1.13	5900	0.84	25
P*t*BA−PS_{96}	1.16	12600	0.23	96
P*t*BA−PS_{240}	1.14	27900	0.088	240

[a] The symbols *n* and *m* denote the number of repeat units for P*t*BA and PS, respectively.

solvent[10−13] or domains formed in a block copolymer solid.[14−16] In addition to the use of block copolymers, homopolymers such as poly(vinyl alcohol)[17,18] or random copolymers containing thiol groups[19] have also been used as the stabilizer for metal or metal oxide nanoparticles. In the latter cases, the homopolymer chains are grafted onto the particles by loop formation. Since the loop length varies only slightly with the contour length of the polymer chain, it may thus be difficult to adjust over a large range the thickness of the homopolymer shell layer. Other methods to graft polymer chains onto the surface of nanoparticles include the replacement of low-molar-mass stabilizers on preformed metal nanoparticles by multidentate polymer chains[20] or the growing of polymer chains from particle surfaces by atom transfer radical polymerization (ATRP).[21]

II. Experimental Section

Materials. Trioctyl phosphine (TOP, 90%), phenyl ether (99%), octyl ether (99%), 1,2-dodacanediol (90%), cobalt acetate tetrahydrate [$Co(OOCCH_3)_2{\cdot}4H_2O$, 98%] were all used as received from Aldrich. Four PAA−PS samples were used in this project. They were obtained from hydrolysis of P*t*BA−PS, where P*t*BA denotes poly(*tert*-butyl acrylate). The diblocks P*t*BA−PS were prepared by atom transfer radical polymerization (ATRP) as described in the Supporting Information. The P*t*BA block consisted of 21 *t*BA units as determined by end group analysis using ^{1}H NMR. The polydispersity index defined as the weight- to number-average molar mass ratio M_w/M_n was measured for this sample by size exclusion chromatography (SEC) based on PS standards to be 1.14. Characteristics of the P*t*BA−PS samples are summarized in Table 1.

Co Nanocrystal Preparation. All reactions were performed in a 50-mL three-neck round-bottom flask under nitrogen protection. In an example run, we started by mixing 5 mL of phenyl ether with 53 mg of $Co(OOCCH_3)_2{\cdot}4H_2O$ (0.213 mmol, 0.025 M in the final solution at a volume of 8.5 mL) and 118 mg of PAA−PS_{96} (0.213 mmol of carboxyl group). The mixture was then heated to 200 °C before 98 μL of TOP (0.213 mmol) was injected. The temperature was held at 200 °C for 1 h with N_2 bubbling to ensure moisture removal. In the meantime, 616 mg of dodecanediol dissolved in 3.6 mL of phenyl ether and 1.4 mL of octyl ether was heated also at 200 °C for 1 h with N_2 bubbling to remove moisture before cooling to 80 °C. By this stage, temperature in the main reaction flask was increased to 240 °C and N_2 bubbling was stopped but a positive pressure maintained. An aliquot of the reductant solution, 3.5 mL containing 2.13 mmol of dodacanediol, was taken and injected into the main flask. The system color changed from deep blue to dark within 10 min. After a total of 2 h, the reaction was terminated by cooling the mixture to room temperature.

Co Nanocrystal Purification. Methanol, ~25 mL, was dropped slowly into a reacted mixture under stirring to precipitate the cobalt nanoparticles. As TOP, dodecanediol, and $Co(OOC\ CH_3)_2{\cdot}4H_2O$ were all soluble in methanol and free PAA−PS formed micelles in phenyl ether/methanol, the excess reactants and surfactants were readily separated from the nanoparticles by centrifugation at 1100*g* for 5 min. The black precipitate was re-dispersed in 2 mL of toluene and separated as a precipitate by adding 6 mL of methanol and centrifugation again. This procedure was repeated another two times to purify the sample. The precipitate was vacuum-dried at room temperature to determine the yield. To test the stability of the adsorbed diblock layer against solvent rinsing, the samples were rinsed more times with toluene or THF.

Co Nanocrystal Fractionation. The purified cobalt nanoparticles (about 30 mg) were dissolved in 10 mL of toluene. Under vigorous stirring methanol was dropped in slowly. Methanol addition was stopped at ~38 vol % when cloudiness was noticed. The solution was left in a refrigerator at −12 °C overnight. The solution was separated into two phases. The bottom denser layer was separated as fraction 1. Additional methanol was added to the dilute phase until the solution became cloudy (methanol volume fraction about 50%). Repeating the procedure described above, we obtained fraction 2 as the bottom denser layer and fraction 3 as the top layer.

Co Nanocrystal Characterization. The particles were aspirated on a nitrocellulose-covered copper grid before observation by transmission electron microscopy (TEM). TEM images were obtained using a Hitachi H-7000 instrument operated at 75 kV. To enable visualization of the PAA−PS shell, the samples were stained with RuO_4 vapor for 1 h. Thermal gravimetric analyses (TGA) were carried out on a TA Q-500 instrument. A typical run consisted of raising the temperature from room temperature to 600 °C at 20 °C/min and then holding the temperature at 600 °C for 20 min.

One Co particle sample stabilized by PAA−PS_{96} with TEM core diameter $d = (9.2 \pm 1.4)$ nm was used for X-ray diffraction study. The sample was dissolved in toluene and dropped on a microscope slide cover slip to evaporate solvent. This procedure was repeated several times to prepare a film that was ~15 μm thick. The X-ray diffraction experiment was performed on Rigaku Ru 200b instrument using the Cu Kα ($\lambda = 1.5418$ Å) radiation.

Small angle neutron scattering measurements were performed at the Argonne National Laboratory using a time-of-flight instrument. The range of scattering wave vector q used was between 0.007 and 1.45 Å^{-1}. Here $q = (4\pi/\lambda)\sin(\theta/2)$ with θ denoting the scattering angle and λ the neutron wavelength. The sample to detector distance used was 1.44 m. The detector had a hemispherical shape consisting of 50 × 50 1-cm^2 area detectors. The samples were prepared in deuterated THF (THF-d_8) at the Co/PAA−PS_{96} concentrations of 2.1, 4.9, or 11.9 wt %, respectively. The path length of the cylindrical cells used was either 1.00 or 2.00 mm and the data acquisition time ranged from 4 to 6 h. The raw intensities were corrected for background scattering by subtracting scattering

(16) For references on metal or metal oxide loading after selective domain degradation see, for example, (a) Liu, G. J.; Ding, J. F.; Hashimoto, T.; Saijo, K.; Winnik, F. M.; Nigam, S. *Chem. Mater.* **1999**, *11*, 2233. (b) Thurn-Albrecht, T.; Schotter, J.; Kastle, G. A.; Emley, N.; Shibauchi, T.; Krusin,-Elbaum, L.; Guarini, K.; Black, C. T.; Tuominen, M. T.; Russell, T. P. *Science* **2000**, *290*, 2126. (c) Hashimoto, T.; Tsutsumi, K.; Funaki, Y. *Langmuir* **1997**, *13*, 6869.
(17) (a) Mayer, A. B. N. *Polym. Adv. Technol.* **2001**, *12*, 96. (b) Hirai, H.; Toshima, N. In *Catalysis Metal Complexes, Tailored Metal Catalysts*; Iwasawa, Y., Ed.; Reidel Publishing Company: Dordrecht, 1986.
(18) (a) Mayer, A. B. R.; Mark, J. E. *Macromol. Rep.* **1996**, *A33*, 451. (b) Hirai, H.; Chawanya, H.; Toshima, N. *React. Polym.* **1985**, *3*, 127.
(19) (a) Teranishi, T.; Kiyokawa, I.; Miyaka, M. *Adv. Mater.* **1998**, *10*, 596. (b) Wuelfing, W. P.; Gross, S. M.; Miles, D. T.; Murray, R. W. *J. Am. Chem. Soc.* **1998**, *120*, 12696. (c) Corbierre, M. K.; Cameron, N. S.; Sutton, M.; Mochrie, S. G. J.; Lurio, L. B.; Ruhm, A.; Lennox, R. B. *J. Am. Chem. Soc.* **2001**, *123*, 10411.
(20) (a) Wang, X. S.; Dykstra, T. E.; Salvador, M. R.; Manners, I.; Scholes, G. D.; Winnik, M. A. *J. Am. Chem. Soc.* **2004**, *126*, 7784.
(21) Ohno, K.; Koh, K.; Tsujii, Y.; Fukuda, T. *Angew. Chem., Int. Ed.* **2003**, *42*, 2751.

Table 2. Parameters Affecting the Size of the Co Nanoparticles

sample	$[Co^{2+}]$/ M	[COOH]/ M	[COOH] /[TOP]	rxn t/h	yield	y_{Co}	TEM Co ($d \pm \sigma$) (nm)	TGA polymer content
				PAA−PS_{25}				
1	0.025	0.025	1/1	2	46.9%		10.4 ± 2.6	
				PAA−PS_{96}				
2	0.0125	0.0125	1/1	2	31.7%		9.2 ± 1.4	
3	0.025	0.025	1/1	2	33.4%		9.6 ± 1.6	
4	0.050	0.050	1/1	2	32.6%	98%	9.6 ± 2.1	63.0%
5	0.025	0.025	2/1	2	32.5%		10.6 ± 1.8	
6	0.025	0.025	4/1	2	34.7%		13.2 ± 2.1	
7	0.025	0.025	4/0	2	no rxn			
8	0.025	0.0125	1/1	2	53.5%		11.4 ± 3.6	
9	0.025	0.025	1/1	0.5	21.7%	33%	4.3 ± 1.0	80.8%
10	0.025	0.025	1/1	1	26.1%	72%	8.2 ± 1.4	65.6%
11	0.025	0.025	1/1	3	31.5%		9.4 ± 1.7	
12	0.025	0.025	1/1	4	31.8%		9.4 ± 1.9	
				PAA−PS_{240}				
13	0.025	0.025	1/1	2	20.4%		7.3 ± 1.3	

from solvent and sample cell.[22] The isotropic scattering intensities were then azimuthally averaged and converted to macroscopic scattering cross sections per unit volume $d\Sigma/d\Omega$ using a correction factor obtained from running the incoherent scatterer water.[23]

Co Nanocrystal Film Preparation. A film was prepared from Co/PAA−PS_{240} by casting a toluene solution of this sample on a microscope slide cover slip directly. To prepare a film from a Co/PAA−PS_{96} sample possessing a TEM core diameter of (9.6 ± 2.1) nm, 20 mg of this sample was dissolved in 2 mL of toluene together with 20 mg of a PS sample (Polysciences, M_w = 20000 g/mol, M_w/M_n = 1.03). An aliquot of the solution was then dropped over an area of ~1 cm^2 on a microscope slide cover slip. After solvent evaporation, another aliquot was dropped on the top of the film. This procedure was repeated until the solution was completely cast.

III. Results and Discussion

Co/PAA−PS Nanoparticle Preparation. Co nanoparticles were prepared by reducing cobalt acetate with dodecanediol in phenyl ether at 240 °C using PAA−PS and TOP as the surfactant and cosurfactant, respectively. The major modification to a literature method involved the replacement of the surfactant oleic acid, used by Sun et al.,[2] by PAA−PS. For the multidentate nature of this new surfactant and thus its stronger binding toward Co, Co^{2+} reduction was slower. Thus, we increased the reaction time from 20 min reported in the literature[2] to typically 2 h. To increase reaction rate further, we increased also the reducing agent dodecanediol amount from 1 to 10 molar equiv relative to Co^{2+}. Table 2 summarizes the recipes used for 13 preparations, where $[Co^{2+}]$, [COOH], and [TOP] denote the molar concentration of Co^{2+}, the carboxyl groups, and TOP in the preparation mixture. Also reported are some properties of the crude particles before fractionation that include the TEM Co particle diameter d and its deviation σ, the polymer content in the particles determined from TGA, reaction yields defined as the ratio between the weight of the final product to that of the initial polymer plus Co^{2+}, and the Co(II) conversion defined as

$$y_{Co} = \frac{w_{Co}}{w_{Co^{2+}}} \quad (1)$$

where w_{Co} and $w_{Co^{2+}}$ are the masses of the produced Co and the initial Co^{2+}, respectively. There is no entry in the table for PAA−PS_6 as the PS block was too short for this diblock to function as an effective surfactant and its use led to the production of aggregated Co particles.

Nanoparticle Size Control. Figure 1 shows the TEM images for samples 9, 3, and 6 with the preparation conditions given in Table 2. Since the samples were not stained, only the Co cores are visible in these images. From TEM images like these we measured manually the diameter of more than 150 Co nanoparticles for each sample and obtained $d \pm \sigma$ with results shown in Table 2. For particles that were asymmetric, the diameter was taken as the average of lengths measured along the long and short axes of the particles.

Samples 9, 10, 3, 11, and 12 were prepared under otherwise identical conditions but with reaction times of 0.5, 1, 2, 3, and 4 h, respectively. The $d \pm \sigma$ values for these samples are 4.3 ± 1.0, 8.2 ± 1.4, 9.6 ± 1.6, 9.4 ± 1.7, and 9.4 ± 1.9 nm, respectively. The data suggest that the size of the particles increased initially with reaction time and remained unchanged after ~2 h. For this we terminated most preparations at 2 h. Considering that samples 11 and 12 are from different batches, the agreement between the $d \pm \sigma$ values for these samples suggest high reproducibility of the preparations.

Other than variations in TOP concentration or [TOP], the preparation conditions for samples 3, 5, 6, and 7 were identical. The d values increased initially with decreasing [TOP]. Then, surprisingly, Co^{2+} failed to reduce if no TOP was added at all. In another experiment we demonstrated that the reaction did not occur even with TOP addition but with it being added only after dodecanediol had been added at 240 °C. Thus, both the presence and the adding sequence of TOP were important to effect Co nanoparticle formation. This size dependence on [TOP] is the opposite of the trend observed by Murray et al.[2b] When oleic acid was used as the surfactant, Co particle size increased with [TOP].

The particle size can also be changed by varying $[Co^{2+}]$/[COOH] or PS block length. Decreasing [COOH] by half

(22) Thiyagarajan, P.; Epperson, J. E.; Crawford, R. K.; Carpenter, J. M.; Klippert, T. E.; Wozniak, D. G. *J. Appl. Crystallogr.* **1997**, *30*, 280.
(23) Higgins, J. S.; Maconnachie, A. In *Methods of Experimental Physics − Neutron Scattering: Vol. 23, Part C*; Skold, K., Price, D. L., Eds.; Academic Press: Orlando, 1987.

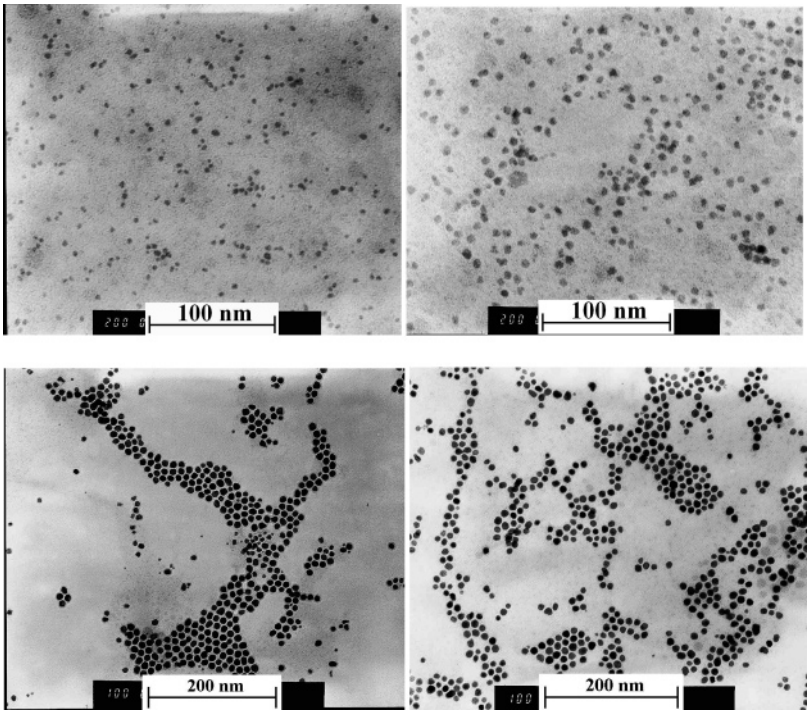

Figure 1. TEM images of samples 9 (top left), 3 (top right), and 6 (bottom left). The bottom right image is for fraction 2 of sample 6 where the smaller particles were seen mostly removed.

from sample 3 to sample 8, the size of the Co particles increased from 9.6 ± 1.6 nm to 11.4 ± 3.6 nm. This was unfortunately accompanied by a broadening in particle size distribution. Increasing the PS block length from 25 units to 96 and 240 units decreased the particle size from 10.4 ± 2.6 to 9.6 ± 1.6 and 7.3 ± 1.3 nm for samples 1, 3, and 13, respectively. Interestingly, the particle size changed insignificantly with the absolute $[Co^{2+}]$ or [COOH] values for samples 2−4 at $[Co^{2+}]/[COOH] = 1$.

Reaction Yield. The reaction yields of column 6 in Table 2 appear low because only a fraction of the added polymer was grafted onto the final Co particle surfaces. To evaluate Co conversion, we determined $w_{Co}{}^{2+}$ of eq 1 readily from the reactant stoichiometry. The determination of w_{Co} required a method to analyze the Co content in Co/PAA−PS. We used TGA for this purpose. To calculate the Co weight fraction from the TGA data, we assumed that the grafted PAA−PS chains decomposed analogously as the free PAA−PS chains and Co survived the thermal decomposition process intact. This allowed us to calculate the Co content using an equation that we derived before[13d] for samples 9, 10, and 4. The y_{Co} values thus determined were 43%, 92%, and 124%, respectively. The y_{Co} value increased with reaction time as expected.

The fact that y_{Co} was higher than 100% for sample 4 suggests our assumption about the inertness of Co nanoparticles was incorrect. If we remove this assumption and assume that all Co atoms reacted with PAA to form CoO during TGA analysis, the y_{Co} values for samples 9, 10, and 4 change to 33%, 72%, and 98%, respectively. The fact that $y_{Co} = 98\%$ for sample 4 suggests that Co might have indeed been fully oxidized by reaction with PAA, a conclusion that remains to be confirmed by a future X-ray diffraction analysis.

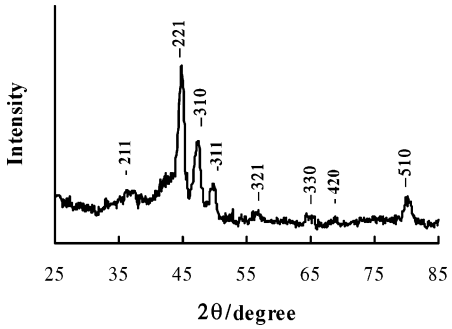

Figure 2. X-ray diffraction data of the Co/PAA−PS_{96} nanoparticles.

Co-Crystal Structure. Co is traditionally known to have two crystal phases: close-packed hexagonal (hcp) and face-centered cubic (fcc). The reduction of $Co(OOCCH_3)_2$ with dodecanediol employing oleic acid as the surfactant yielded hcp Co nanocrystals.[2b] The thermal decomposition of $Co_2(CO)_8$ in phenyl ether/ octyl ether using oleic acid and TOP as the surfactants yielded fcc Co nanocrystals.[2c] More recently, Dinega and Bawendi[3b] discovered the ϵ-Co crystal phase for Co nanoparticles. This phase has since also been seen by Puntes et al.[3a] and Sun et al.[2a]

Illustrated in Figure 2 are the X-ray diffraction data of sample 2. The peak positions and peak intensity distribution bear exact resemblance to that reported for ϵ-Co nanoparticles.[3a,b] We have thus produced ϵ-Co nanoparticles.

The half-maximum widths $\delta_{2\theta}$ for the (221) and (310) peaks in Figure 2 are 1.10 and 1.12°, respectively. Assuming that the small size of the cobalt particles was the dominant cause for peak broadening, we used these $\delta_{2\theta}$ values in the Scherrer equation

$$d_X = \frac{K\lambda}{\delta_{2\theta}\cos\theta} \qquad (2)$$

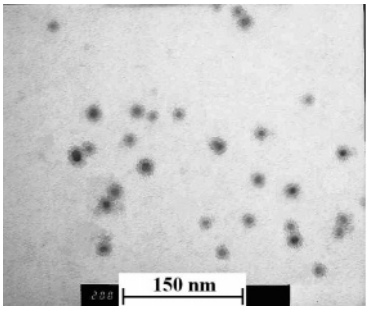

Figure 3. TEM image of F2 of sample 8 with core and shell clearly distinguishable.

Table 3. Effect of Co Nanoparticle Fractionation

sample	TEM ($d \pm \sigma$)/nm	weight fraction
sample 8	11.4 ± 3.6	100%
F1	12.8 ± 2.5	43%
F2	11.2 ± 1.9	35%
F3	10.3 ± 2.3	19%
sample 6	13.2 ± 2.1	100%
F1	13.6 ± 1.9	~10%
F2	13.4 ± 1.0	~50%
F3	12.9 ± 1.8	~40%

to calculate the average diameter d_X of the particles, where $\lambda = 0.15418$ nm.[24] To assign the K value, we assumed that the particles were approximately spherical and thus $K = 1.107$. This yielded a d_X value of 9.3 nm from both peaks. This is in good agreement with the TEM diameter of (9.2 ± 1.4) nm, suggesting that the particles produced were single crystals.

Fractionation. Our examination of different batches of Co/PAA−PS_{96} nanocrystals including those not listed in Table 2 led to the conclusion that they became visually nondispersible at diameters greater than ~15 nm. Below this size, particles even after being dried under vacuum could be re-dispersed in solvents good for PS. The dispersed particles could be fractionated by fractionation precipitation following procedures described in the Experimental Section.[2,3] Table 3 shows the characteristics of samples 8 and 6 before and after fractionation. The effectiveness of the fractionation procedure is evident as judged from the changes in the TEM d and σ value for different fractions.

Compared in Figure 1 are the TEM images of sample 6 and fraction 2 of this sample. The smaller particles were obviously removed from the fractionated sample. The relative spread in d or σ/d was ~7.5% for this sample and could in principle be further reduced by repeating the fractionation procedure.

Core−Shell Structure. We were able to discern by TEM the PAA−PS layer on the Co nanoparticles when the samples were stained by RuO_4. Figure 3 shows a TEM image with core−shell structure clearly visible for fraction 2 of sample 8 (Table 3). Magnifying pictures like this, we measured manually the thickness of the PAA−PS layer around many particles. This yielded the average shell thickness of 5.7 nm for this sample. Similarly, we determined a thickness of 14 nm for sample 13. Thus, the shell thickness increased with PS chain length as anticipated.

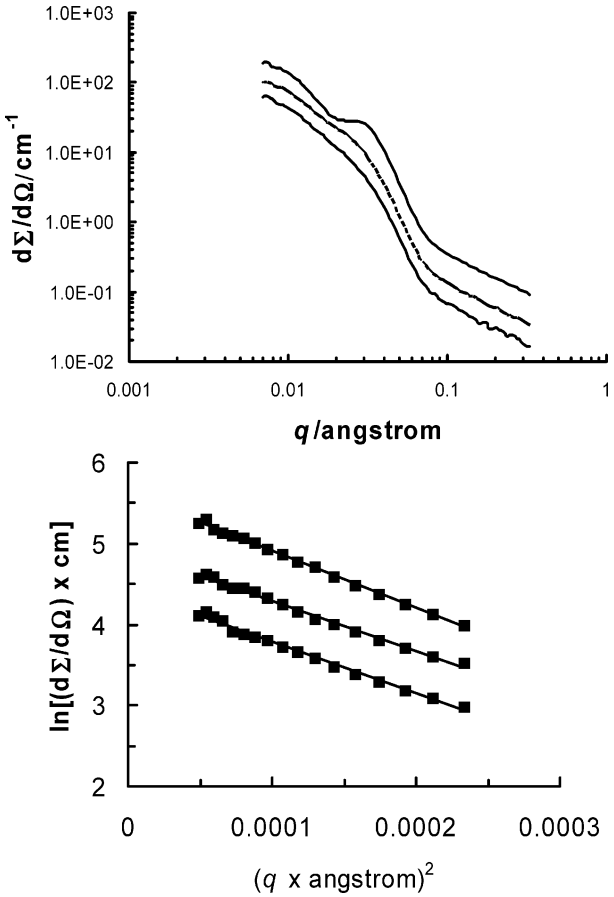

Figure 4. Top panel: neutron scattering data of a Co/PAA−PS_{96} sample at the concentrations of 11.4% (top curve), 4.9% (middle), and 2.1% (bottom). Bottom panel: Guinier plots of the neutron scattering data in the region with $q < 0.0153$ Å. From top to bottom, the particle concentration decreased.

Table 4. Effect of Solvent Rinsing on the Stability of the Grafted PAA−PS_{96}

sample	treatment	grafted polymer content
4	rinsed 3 times with toluene	63.0%
4	rinsed 5 times with toluene	63.5%
8	rinsed 3 times with toluene	59.9%
8	rinsed 3 times with toluene and 3 times with THF	45.2%
8	rinsed 3 times with toluene and 5 times with THF	42.8%

Further support for the core−shell structure was rendered by comparing for one sample the TEM Co particle size and its radius of gyration R_G value. We determined the R_G value from neutron scattering because the hybrid particles were dark and absorbed laser light and neutron scattering is a technique that is much less sensitive to optical opacity. The top panel in Figure 4 shows the neutron scattering data for a Co/PAA−PS_{96} sample with ($d \pm \sigma$) = (11.4 ± 2.7) nm at the concentrations of 2.1, 4.9, and 11.4 wt %. Aside from the data at 11.4%, the other two sets of data bear much resemblance in shape. It has been long known that[25]

$$\frac{d\Sigma}{d\Omega} = \mathcal{N}P(q)S(q) \qquad (3)$$

(24) Klug, H. P.; Alexander, L. E. *X-ray Diffraction Procedures for Polycrystalline and Amorphous Materials*; John Wiley & Sons: New York, 1954.

(25) Garamus, V. M.; Maksimova, T.; Richtering, W.; Aymonier, C.; Thomann, R.; Antonietti, L.; Mecking, S. *Macromolecules* **2004**, *37*, 7893.

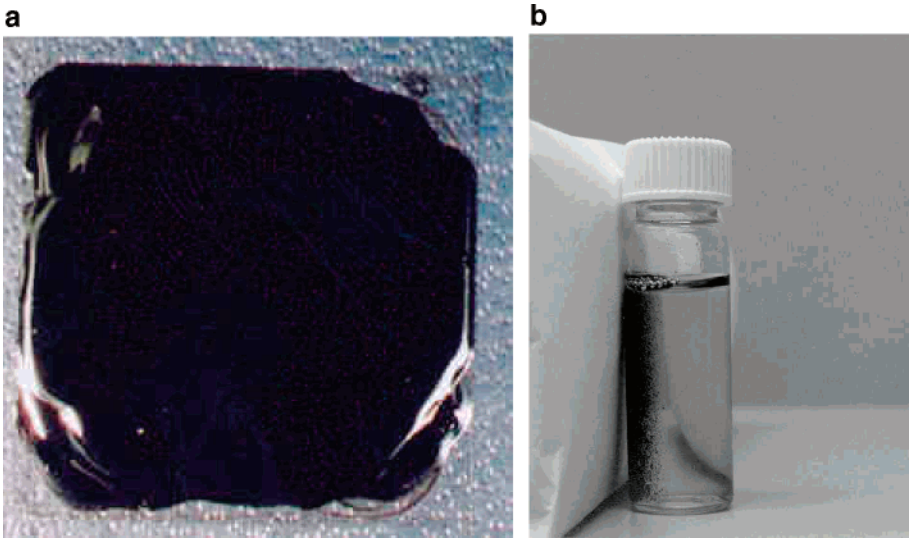

Figure 5. Photographs demonstrating (a) film formation from a Co/PAA−PS_{96} nanoparticle sample and (b) the capturing of small pieces of a Co/PAA−PS_{96} nanoparticle film.

where $\mathcal{N}$ is the number density of particles, $P(q)$ is the form factor of particles describing the size and shape of one individual particle, and $S(q)$ is the structure factor describing the long-range organization of the different particles. The $d\Sigma/d\Omega$ data of the most concentrated sample had new features because some form of particle organization has set in. For the more dilute samples, $S(q) \approx 1$.

Sophisticated models exist for the treatment of the $d\Sigma/d\Omega$ data of core−shell particles to yield parameters such as the core size and shell thickness etc.[26] As far as this synthesis paper is concerned, we treated the scattering data only by a model-free method or the Guinier method in the low q region where $qR_G < \sim 1$. In Guinier's approximation

$$\ln\left(\frac{d\Sigma}{d\Omega}\right) = -(1/3)R_G^2 q^2 + \ln\left(\frac{d\Sigma(0)}{d\Omega}\right) \qquad (4)$$

where $d\Sigma(0)/d\Omega$ is the extrapolated macroscopic scattering cross section per unit volume at $\theta = 0$. The bottom panel in Figure 4 plots the data following eq 4 in the region with $q < 0.0153$ Å. From the slope we obtained R_G of 13.7, 13.7, and 13.9 nm at the particle concentrations of 2.1%, 4.9%, and 11.4%, respectively. The agreement between the R_G values obtained at lower concentrations again suggests the negligible $S(q)$ contribution to $d\Sigma/d\Omega$ in these cases.

The neutron scattering diameter of gyration d_G of 27.4 nm is larger than d_{TEM} of (11.4 ± 2.7) nm. This is reasonable as TEM gives the diameter of the Co core only and d_G offers a measure of the overall size of the particles including the grafted PAA−PS chains. Assuming the full stretching of the grafted PS chains, we estimated an overall diameter d of ~60 nm for the particles. For a homogeneous sphere $d_G = \sqrt{3/5}d$. Our d_G value should be less than $\sqrt{3/5}d$ or ~46 nm and is equal to 27.4 nm as the PS chains are not fully stretched and the Co core is more dense than the PS corona.

Stability of the Adsorbed PAA−PS Layer. The Co nanoparticle samples were purified using procedures described in the Experimental Section, which involved precipitation initially from the reaction medium or later from toluene three times by methanol addition. We repeated the precipitation purification procedure another two times for sample 4. Table 4 gives the TGA analysis results for sample 4 rinsed by toluene for different times. After the sample was rinsed five times with toluene, TGA detected a grafted polymer content of 63.5%, which was, within experimental error, the same as 63.0% determined for the sample after toluene rinsing three times. This shows the superb stability of the adsorbed layer against toluene rinsing.

We also checked the effect of THF rinsing on the stability of the adsorbed layer. Unlike toluene that solubilizes only the PS block, THF solubilizes both the PS block and the short PAA block and should remove most of the PAA−PS chains if not for the strong binding between PAA and Co. After sample 8 was rinsed with toluene three times, it had a grafted polymer content of 59.9%. This number reduced to 45.2% after rinsing three more times with THF. The number further reduced to 42.5% after THF rinsing two more times. Thus, the THF removal rate decreased with increasing number of THF rinsings probably due to the fact that the equilibrium adsorbed PAA−PS amount in THF was reached after rinsing in THF three times or less. Despite the sample being rinsed five times in THF, the particles dispersed superbly well in THF.

For comparative purposes, we prepared also Co nanocrystals with a diameter of 8.4 ± 1.1 nm coated by oleic acid. After the precipitation of the particles from the initial reaction mixture into methanol, the particles were easily re-dispersed in THF. We precipitated the particles again by adding methanol. Unfortunately, a large fraction of particles became nondispersible in THF. Repeating the methanol addition and precipitation procedure another time, the particles became totally nondispersible in THF. These results demonstrate that

(26) (a) Vangeyte, P.; Leyh, B.; Heinrich, M.; Grandjean, J.; Bourgaux, C.; Jerome, R. *Langmuir* **2004**, *20*, 8442. (b) Pedersen, J. S.; Svaneborg, C.; Almdal, K.; Hamley, I. W.; Young, R. N. *Macromolecules* **2003**, *36*, 416. (c) Won, Y.-Y.; Davis, H. T.; Bates, F. S.; Agamalian, M.; Wignall, G. D. *J. Phys. Chem. B* **2000**, *104*, 7134. (d) Stancik, C. M.; Lavoie, A. R.; Achurra, P. A.; Waymouth, R. M.; Gast, A. P. *Langmuir* **2004**, *20*, 8975.

the polymer-coated particles are much more stable toward solvent rinsing than the oleic-acid-coated particles.

Film Formation and Magnetic Property. An anticipated advantage of polymer-coated Co nanocrystals is their readiness for film formation. For sample 13 coated by PAA−PS_{240}, we were able to cast intact films directly from a toluene dispersion of the particles. Unfortunately, films formed from particles coated by PAA−PS_{96} were cracked for the low polymer volume fraction in these samples. This was, however, readily remedied by mixing the samples with some PS homopolymer. Figure 5a shows a photograph of a Co nanoparticle film prepared from casting a mixture of sample 4 and a polystyrene homopolymer at the mass ratio of 1/1 from toluene on a microscope cover slip. The freshly prepared film bears the dark color and metallic luster of Co as expected.

To see if the particles were magnetic, we ground up a film cast from a Co/ PAA−PS_{96} sample. The particles were ultrasonicated in water and then placed next to a 0.47-T magnet. The attraction and concentration of the particles by the magnet demonstrates that they were either superparamagnetic or ferromagnetic.

IV. Conclusions

We have prepared PAA−PS diblock copolymers with 21 AA units and different lengths for the PS block. Aside from the sample with only 6 styrene units, the other samples with 25, 96, and 240 styrene units functioned well as surfactants in the one-pot synthesis of Co nanoparticles. The Co nanoparticles were prepared via high-temperature reduction of Co(II) by dodecanediol using TOP as the cosurfactant. The size of the particles could be tuned by changing various parameters including the reaction time and TOP concentration etc. The lattice structure of the nanocrystals was determined by X-ray diffraction to be ϵ-Co. The size distribution of the crude Co nanoparticles could be narrowed down by fractionation precipitation. Due to the multidentate nature of PAA, the adsorbed PAA−PS chains were very resistant to solvent rinsing. As expected, the polymer-coated Co nanocrystals were readily cast into mechanically robust films bearing metallic luster provided that the PS coating block was sufficiently long at 240 repeat units.

Acknowledgment. NSERC of Canada is gratefully acknowledged for sponsoring this research. G.J.L. thanks the Canada Research Chairs Program for a chair position in materials science.

Supporting Information Available: Preparation and characterization of PAA−PS. This material is available free of charge via the Internet at http://pubs.acs.org.

CM051050B